Eur Radiol (2003) 13:195–208
DOI 10.1007/s00330-002-1524-x

EXPERIMENTAL

Vasilis Ntziachristos
Christoph Bremer
Ralph Weissleder

Fluorescence imaging with near-infrared light: new technological advances that enable in vivo molecular imaging

Received: 23 March 2002
Accepted: 15 April 2002
Published online: 19 July 2002

V. Ntziachristos (✉) · C. Bremer
R. Weissleder
Center for Molecular Imaging Research,
Massachusetts General Hospital
and Harvard Medical School,
Building 149, 13th Street 5406,
Charlestown MA 02129–2060, USA
e-mail: vasilis@helix.mgh.harvard.edu
Tel.: +1-617-7266091
Fax: +1-617-7265708

Abstract A recent development in biomedical imaging is the non-invasive mapping of molecular events in intact tissues using fluorescence. Underpinning to this development is the discovery of bio-compatible, specific fluorescent probes and proteins and the development of highly sensitive imaging technologies for in vivo fluorescent detection. Of particular interest are fluorochromes that emit in the near infrared (NIR), a spectral window, whereas hemoglobin and water absorb minimally so as to allow photons to penetrate for several centimetres in tissue. In this review article we concentrate on optical imaging technologies used for non-invasive imaging of the distribution of such probes. We illuminate the advantages and limitations of simple photographic methods and turn our attention to fluorescence-mediated molecular tomography (FMT), a technique that can three-dimensionally image gene expression by resolving fluorescence activation in deep tissues. We describe theoretical specifics, and we provide insight into its in vivo capacity and the sensitivity achieved. Finally, we discuss its clinical feasibility.

Keywords Near infrared · In vivo · Molecular imaging · Fluorescence

Introduction

Tissue observation with light is probably the most common imaging practice in medicine and biomedical research ranging from the simple visual inspection of a patient to advanced in vivo and in vitro spectroscopic and microscopy techniques [1]. While intrinsic tissue absorption and scattering yields significant information on functional and anatomical tissue characteristics, significant attention has also been given to fluorescence investigations of tissue since many biochemical markers can be retrieved due to fluorescence contrast, and many more can be targeted using appropriate fluorescent markers [2, 3].

Numerous different optical imaging approaches can be used for imaging fluorescence in vivo. Traditionally, optical methods have been used to look at surface and subsurface fluorescent events using confocal imaging [4, 5, 6], multiphoton imaging [7, 8, 9, 10] microscopic imaging by intravital microscopy [11, 12] or total internal reflection fluorescence microscopy [13]. Recently however, light has been used for in vivo interrogations deeper into tissue using photographic systems with continuous light [14, 15, 16, 17] or with intensity-modulated light [18] and tomographic systems [19, 20]. Potentially, phased-array detection [21] can also be applied. This recent focus in macroscopic observations of fluorescence in tissues has evolved due to the potential of transferring this technology to imaging through animals and humans [2]. This technology has become feasible mainly due to the development of fluorescence probes emitting in the near-infrared spectrum where tissue offers low absorption, highly sensitive detectors and monochomatic light sources (lasers) with higher but nevertheless safely delivered power per wavelength compared with white-light illuminators. While macroscopic fluorescence imaging in the visible has also been attempted using fluorescent proteins, the penetration depth is limited to only 1–2 mm

[16], whereas it has been predicted that NIR fluorescent light can penetrate for several centimeters [22]. Such an approach could enable investigations available currently only for in vitro studies to propagate in in vivo human disease diagnosis and imaging of treatment response and significantly enhance the field of molecular imaging [2].

In this article we discuss imaging techniques that use the diffuse component of light for probing molecular events deep in tissue. Specifically, we focus on reflectance fluorescence imaging and fluorescence-mediated molecular tomography (FMT), which are the two most common approaches currently used for imaging fluorescent probes in deep tissues. We further discuss recent findings that predict the capacity of near-infrared fluorescent signals to propagate through human tissue for non-invasive medical imaging and address feasibility issues for clinical studies.

Reflectance imaging

Technology

Simple "photographic methods", in which the light source and the detector reside on the same side of the animal imaged, are generally referred to as "reflectance imaging". Reflectance imaging is currently the typical method of choice for accessing the distribution of fluorescent probes in vivo, but the method can be applied more generally to imaging fluorescent proteins or even bioluminescence even if in the latter case no excitation light is used [23].

Near-infrared fluorescence reflectance imaging in particular operates on light with a defined bandwidth as a source of photons that encounters a fluorescent molecule ("optical contrast agent or molecular probe"), which emits a signal with different spectral characteristics, that can be resolved with an emission filter and captured by a high-sensitivity CCD camera.

A typical reflectance imaging system is shown in Fig. 1. The light source can be either a laser at an appropriate wavelength for the fluorochrome targeted or white light sources using appropriate low-pass filters. Generally, laser sources are preferable because they offer higher power delivery at narrower and better-defined spectral windows (typically ±3 nm for laser diodes vs ±10 nm or more for filtered white-light sources). The laser beam is expanded on the animal surface with an optical system of lenses (not shown). Narrow wavelength selection is important, especially in the NIR, whereas the excitation and emission spectra overlap and it is likely that excitation photons can propagate into the fluorescent images. The CCD camera is usually a high-sensitivity camera since fluorescent signals are of low strength. On the other hand, since the targeted measurement is a diffuse-light measurement, emanating from a virtually flat surface,

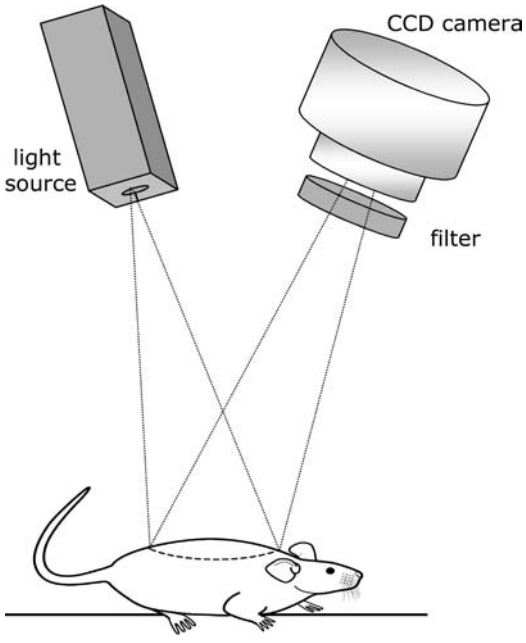

Fig. 1 Typical fluorescence reflectance imaging (FRI) system for in-vivo animal investigations. The illumination source and CCD camera are on the same side of the animal imaged. The components shown are usually enclosed into a light-tight box

CCD chip resolution and dynamic range are not crucial factors in these types of systems. Also the noise requirements of a CCD camera for fluorescence imaging are not as stringent since in the general case the detection sensitivity limit is set by the background tissue fluorescence (background probe distribution and auto-fluorescence), and fluorescence strength can be adjusted above the camera noise floor by optimizing illumination strength and acquisition times. These features are in contrast to bioluminescence measurements, where the detection sensitivity is usually set by the CCD camera noise floor. Detection systems that scan a single spot over a field of view and detect light using photo-multiplier tube detectors have also been reported [24]. Such systems may offer greater dynamic range than CCD-based systems but compromise resolution, acquisition frame rate, and overall noise characteristics, and are not widely used in in vivo fluorescence reflectance measurements.

Typically, the fluorescence image acquired (see example in Fig. 2a) is accompanied by a second image, shown in Fig. 2b, which is measured without the fluorescence filter to obtain a "photograph" of the animal for registration purposes at the excitation wavelength. This intrinsic light image also serves as a calibration measurement since it records the exact spatial distribution of the excitation light strength for later correction of excitation field inhomogeneities. Figure 2 depicts a measurement from a nude mouse with a cathepsin B rich HT1080 fibrosarcoma, which had been implanted (10^5 cells) into

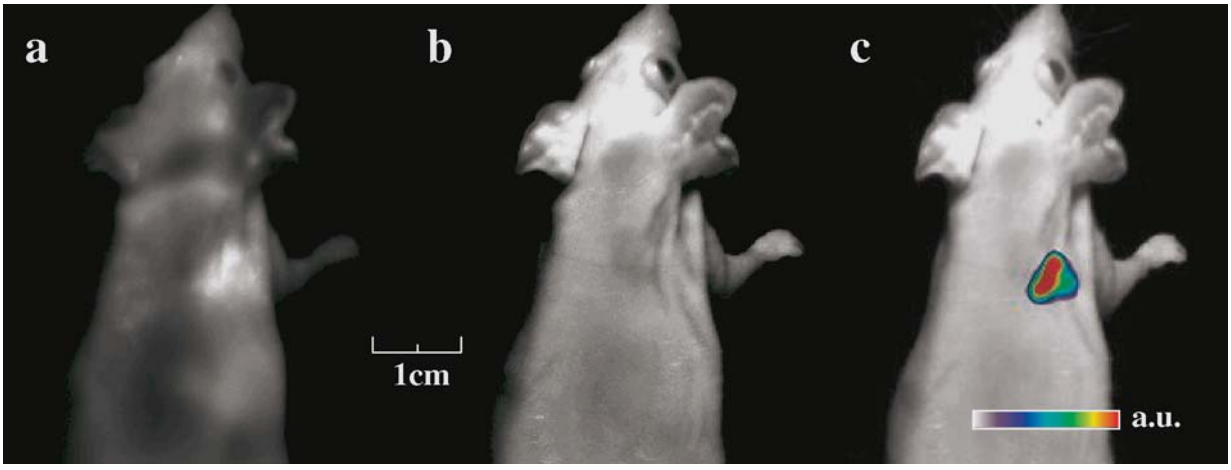

Fig. 2a–c Example of typical images involved in FRI. **a** Fluorescence image obtained from the animal. In this example the image is obtained using a cathepsin-B sensitive fluorescent probe injected in an animal implanted with a HT1080 carcinoma in the upper posterior thorax. **b** Intrinsic light image obtained without the fluorescent band-pass filter. Such images are useful to outline with greater detail the animal investigated. **c** Superposition of **a** onto **b** improves the visual result

the posterior upper thorax of the mouse 7–10 days prior to the experiment, at ~3 mm depth using a cathepsin B sensitive imaging probe [25]. It is noteworthy that the intrinsic light image records the structure on the animal surface and can yield high-resolution images after appropriate focusing, whereas the fluorescence (or luminescence) image records fluorescence signals emanating from under the surface and is by nature a low-resolution image that uses mainly the diffuse component of light. The side-by-side comparison or the superposition of the two images (c.f. Fig. 2c) into a single image yields a good visual effect since high resolution is retained.

Applications

Reflectance imaging has been used to image cathespin B [25], cathepsin D [26] and matrix metalloproteinase 2 (MMP-2) [27] using activatable probes, i.e., appropriately engineered fluorochromes that are dark in their native (quenched) state and fluoresce only upon interaction with specific proteases. A representative mechanism of activation is shown in Fig. 3. In the non-activated state fluorochromes are loaded in closed proximity onto a graft copolymer consisting of a poly-lysine (PL) backbone through appropriate peptides and undergo mutual energy transfer; thus, they exist in a quenched state. At the presence of the targeted enzyme, cleavage of the peptide link releases the fluorochromes which results in a bright fluorescence signal, which can be detected in vivo.

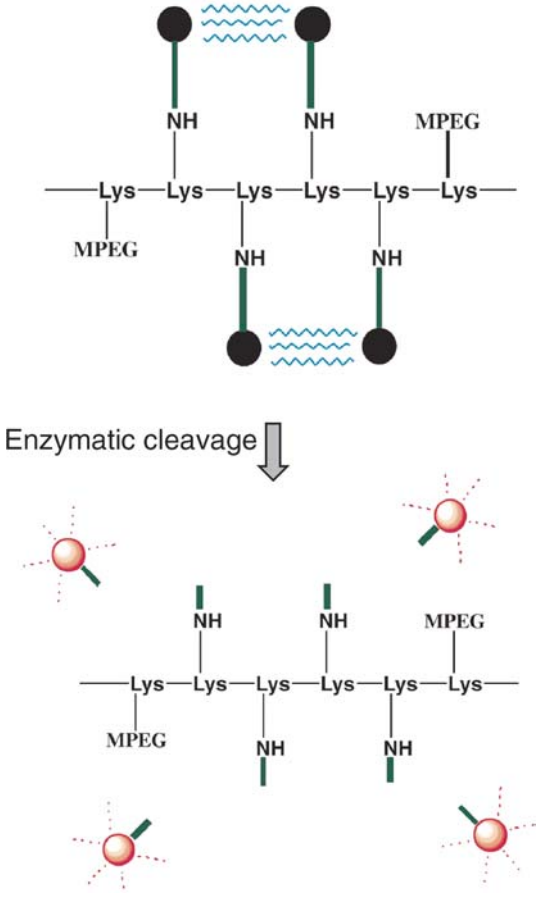

Fig. 3 An example of an activatable probe. These probes are dark in their native state, but after enzymatic cleavage of the backbone carrier they fluoresce when appropriately excited

A characteristic example of this technology applied to elucidate different expression levels of tumor MMP-2 activity is shown in Fig. 4 using an MMP-2-positive human HT1080 fibrosarcoma and an MMP-2-negative BT20 mammary adenocarcinoma [28]. Both types of

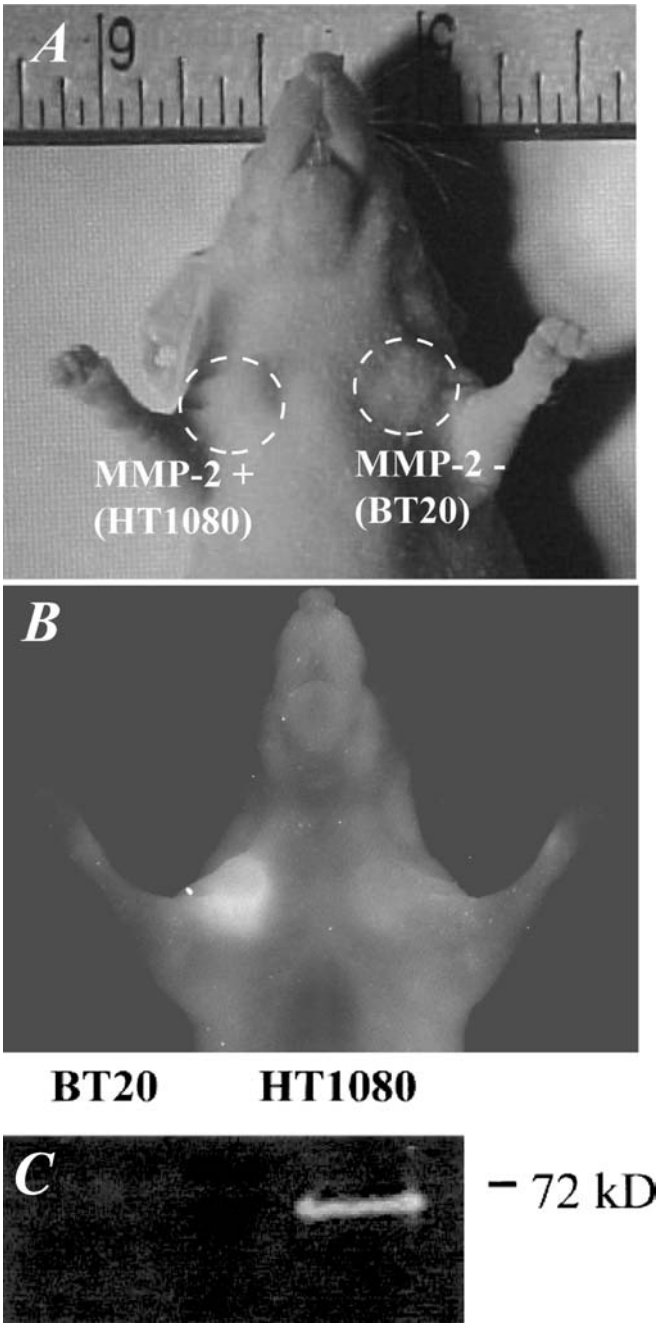

Fig. 4a–c Near-infrared imaging of a nude mouse implanted with both an MMP-2-positive human HT1080 fibrosarcoma and an MMP-2-negative BT20 mammary adenocarcinoma. **a** Both tumors measured approximately 2–3 mm. **b** Raw near-infrared image shows that the fibrosarcoma generated strong fluorescent signal intensity 2 h after intravenous injection of an MMP-2-sensitive activatable probe, but the signal intensity of the BT20 tumor was only slightly higher compared with the background fluorescence of the skin. **c** Zymographic measurements revealed a significant difference between MMP-2 secretions by the two tumor lines. (Adapted from [28])

breast cancers activated the near-infrared probe, but the activation at the HT1080 tumor was markedly higher than the BT-20 tumor which was barely differentiable from the background activation. The different levels of enzyme secretion in the two tumor cell lines used were further verified by zymographic studies [28] as shown in Fig. 4c.

Reflectance imaging has also been used for targeting cell-surface receptors in vivo using peptide near-infrared dye conjugates [15, 29]. Figure 5 depicts fluorescence reflectance images using a conjugate of tricarbocyanine dye and an octapeptide (c.f. Fig. 5a) for targeting the somatostatin receptor in CA20948 tumor-bearing rats [29, 30]. The tumor cells were implanted subcutaneously in the left flank of the rat demonstrating a marked fluorescence increase compared with surrounding tissues (Fig. 5b, c). Similar observations were performed in a separate study [15] that showed significant fluorescence increase from tumor sites compared with normal tissues using the somatostatin analog octreotate coupled to indocarbocyanine dyes. Specifically, the fluorescence detected before the injection of the dye-peptide conjugate administered in a tumor-bearing mouse (RIN38 pancreatic tumor expressing the somatostatin receptor subtype 2) and a control mouse are shown in Fig. 6a and b, respectively. Figure 6c and d show the fluorescence images obtained from the same animals 6 h after probe injection. The administered probe dose was 0.02 μmol/kg body weight. The receptor-binding indotricarbocyanine-octreotate conjugate leads to a significantly elevated tumor signal (Fig. 6c), whereas a control conjugate with no receptor affinity does not generate contrast (Fig. 6d). The relative fluorescence intensities of tumor tissue and normal tissue in the tumors studied with two different dye conjugates are shown in Fig. 6e and f (indodicarbocyanine-octreotate, Fig. 6e; and indotricarbocyanine-octreotate, Fig. 6f) at different times after application. The time course of tumor-to-normal contrast is depicted for both compounds in Fig. 6g. Figure 6h shows the results of a biodistribution analysis of 125I-ITCC-octreotate in RIN38 tumor-bearing nude mice 24 h post injection. Tissue distribution of this double-labeled peptide derivative is given as percentage injected dose per gram.

More generally, reflectance imaging can be used to macroscopically assess endogenous gene products by using fluorescent proteins [16, 31]. Imaging of florescent proteins (FP) can be done in analogy to near-infrared imaging with the following exceptions:

1. Absorption/excitation are shifted in, usually to the visible light range
2. The higher endogenous tissue absorption in the visible wavelength yields significantly smaller penetration depths
3. No exogenous fluorochromes have to be administered to visualize FP expression

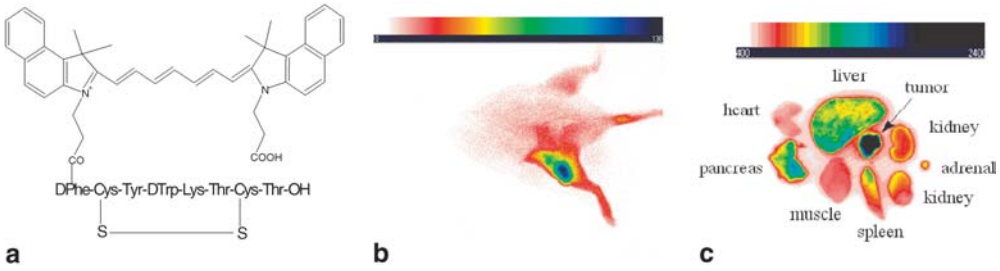

Fig. 5 **a** Molecular structure of cytate, a conjugate of tricarbocyanine dye for near-infrared imaging and an octapeptide for targeting somatostatin receptor which is up-regulated in neuroendocrine tumors. **b** Fluorescence intensity imaging of a CA20948 tumor-bearing rat 27 h post administration of cytate via the tail vein. Tumor cells were implanted subcutaneously in the left flank of the rat. **c** Fluorescence-intensity image of selected organ parts excised 24 h post injection of cytate. The somatostatin receptor-positive tumor, CA20948, preferentially retains cytate. (Adapted from [29] and [30])

In a similar paradigm, bioluminescence imaging [32] is based on emission of visible photons at specific wavelengths based on energy-dependent reactions catalyzed by luciferases. Luciferase genes have been cloned from a large number of organisms, including bacteria, firefly (*Photinus pyralis*), coral (*Renilla*), jellyfish (*Aequorea*), and dinoflagellates (*Gonyaulax*). In the firefly, luciferase utilizes energy from ATP to convert its substrate luciferin to oxyluciferin, with the emission of a detectable photon. Sensitive imaging systems have been built to detect quantitatively a small number of cells or organisms expressing luciferase as a transgene [33].

Multi-spectral imaging

An exciting approach in optical imaging is capitalizing on the spectral differentiation of different fluorochromes in order to perform concurrent imaging of multiple targets [34]. This can be achieved by using appropriate filters in front of the CCD detector that can selectively acquire images at different wavelengths. Figure 7 exemplifies this approach by showing images of GFP and cathepsin B expression obtained from a nude mouse implanted subcutaneously with GFP positive 9L glioma tumors on the right side and GFP negative 9L glioma tumors on the left side [34]. Both tumors were expressing cathepsin B, which was imaged with a cathepsin-B sensitive probe [25] loaded with the Cy5.5 fluorochrome (Amersham Pharmacia Biotech, Piscataway, N.J.). The images were acquired consecutively using appropriate filters in front of the detector for imaging at the GFP spectral window (500–550 nm) and at the Cy5.5 dye channel (690–740 nm) and demonstrate the ability to image separate gene expressions in vivo

Advantages and limitations

Reflectance imaging is an ideal tool for high-throughput imaging and screening of surface fluorescent events in vivo or in excised tissues. It offers simplicity of operation and high sensitivity for molecular events that are close to the surface. Typical acquisition times range from a few seconds to a few minutes. For laboratory settings, multiple animals can be simultaneously imaged. Hardware development and implementation is also straightforward and relatively inexpensive. Reflectance systems do not use ionizing radiation, employ safe laser powers, can be made portable and attain small space requirements to be ideal for the laboratory bench.

On the other hand, reflectance imaging has fundamental limitations both as a research or clinical tool. Firstly, the technique attains only small penetration depths (a few millimeters). This is because the appearance of deeper lesions is significantly blurred and the signal detected from them is significantly attenuated as a function of lesion depth while the background noise remains constant in reflectance mode since it consists of fluorescence signals from superficial layers and intrinsic light contaminating the fluorescence measurement due to imperfect filtering. This is in contrast to tomographic methods (discussed in the next section) where both signal and noise reduces so that signal to noise remains significant for lesions that are much deeper than a few millimeters. Secondly, reflectance imaging is not capable of quantification as illustrated in Fig. 8. A small structure of high fluorochrome concentration that is deeper into tissue could yield the same appearance on the surface as a larger structure of low fluorochrome concentration that is closer to the surface. This is due to the nature of propagation of diffuse photon density waves into tissue. The photon count reading at a surface of an animal due to a lesion on or under the surface depends on the lesion depth, the lesion volume and the optical properties of both the lesion and the surrounding tissue; therefore, images from different animals, or from the same animal at different time points, are generally insufficient for yielding quantitative insights.

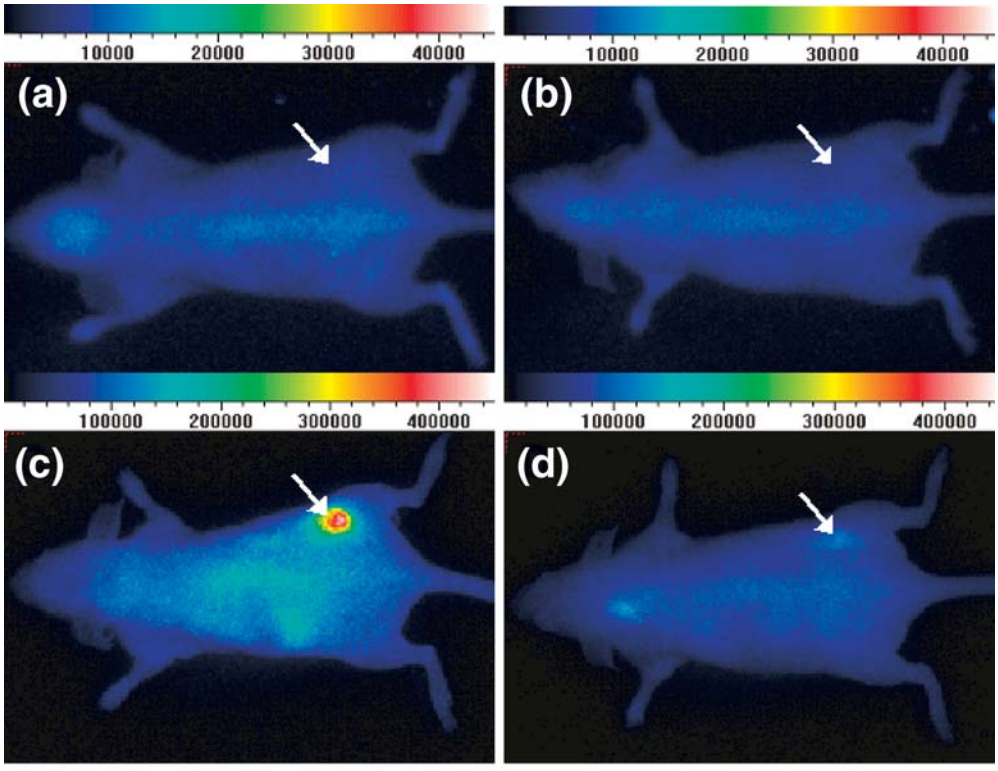

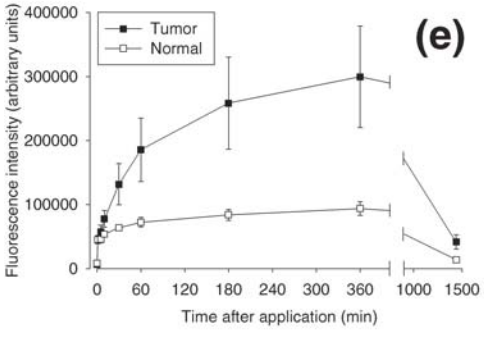

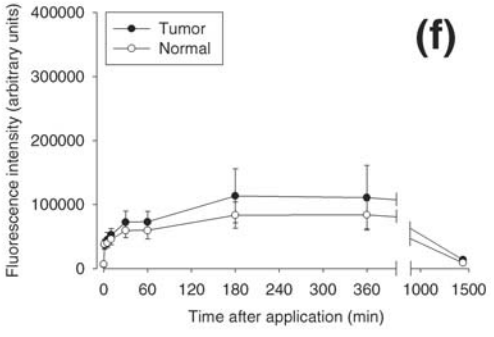

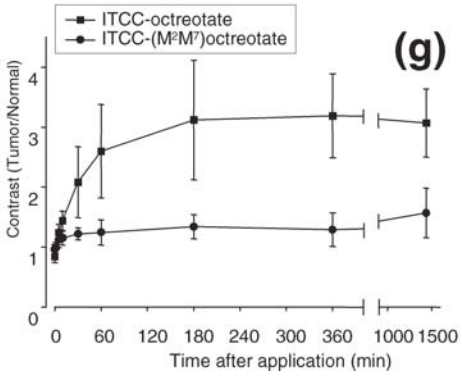

Biodistribution of ^{125}I-ITCC-octreotate

Tissue	*%injected dose/gram*
liver	1.41
kidney	0.41
tumor	0.28
heart	0.12
femur	0.07
muscle	0.04
brain	0.01

(h)

Fig. 6 In vivo fluorescence images of tumor-bearing mice (RIN38 pancreatic tumor expressing the somatostatin receptor subtype 2) **a**, **b** before and **c**, **d** 6 h after injection of dye-peptide conjugate at a dose of 0.02 µmol/kg body weight. **c** The receptor-binding indotricarbocyanine–octreotate conjugate leads to a significantly elevated tumor signal, whereas **d** a control conjugate with no receptor affinity does not generate contrast. Relative fluorescence intensities of tumor tissue and normal tissue in RIN38/SSTR2 tumors from nude mice after intravenous injection **e** of ITCC-octreotate or **f** ITCC-(M2M7) octreotate at different times after application. **g** The time course of tumor-to-normal contrast is depicted for both compounds. **h** The results of a biodistribution analysis of 125I-ITCC-octreotate in RIN38/SSTR2 tumor-bearing nude mice 24 h post injection. Tissue distribution of this double-labeled peptide derivative is given as percentage injected dose per gram. (Image courtesy of K. Licha is taken from [15])

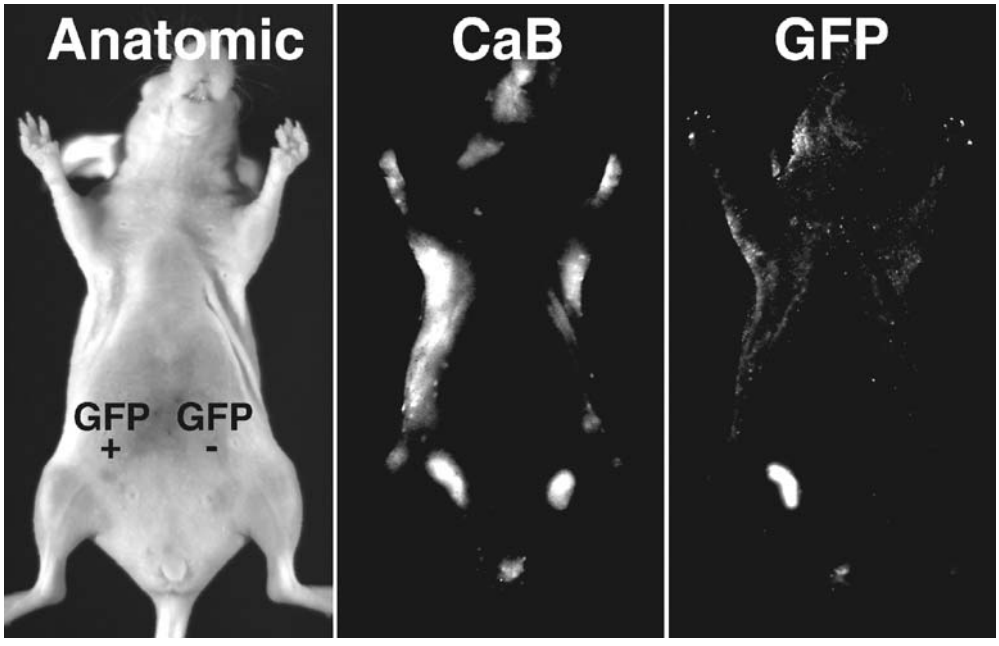

Fig. 7 Dual-channel imaging of genetically identically 9L glioma tumors except for GFP expression (positive on animal's right flank, negative on animal's left flank). Both tumors are expressing cathepsin B. From left to right: white-light image, GFP image, and cathepsin B obtained virtually simultaneously using spectrally separated fluorescence reflectance images. (Image courtesy of U. Mahmood adapted from [34])

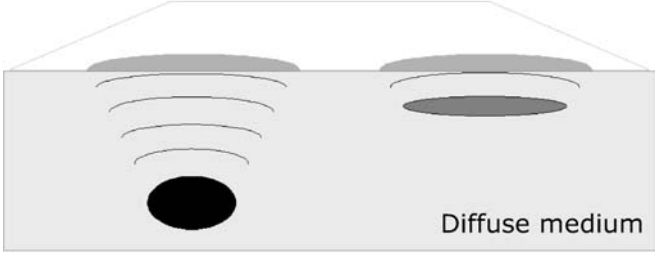

Fig. 8 Different strength and size fluorescent lesions embedded in a diffuse medium at different lengths can have the same appearance on the surface impeding quantification using reflectance imaging

Fluorescence-mediated molecular tomography

In order to resolve and quantify fluorochromes deep in tissue tomographic approaches are necessary. The general framework of reconstruction techniques using diffuse light has been developed during the last decade where rigorous mathematical modeling of light propagation in tissue, combined with technological advancements in photon sources and detection techniques has made possible the application of tomographic principles [35, 36, 37, 38, 39, 40] for optical imaging. The technique, generally termed diffuse optical tomography (DOT), uses multiple projections and measures light around the boundary of the illuminated body. It then effectively combines all measurements into an inversion scheme that takes into account the highly scattered photon propagation to deconvolve the effect of tissue on the propagating wave, even though high frequency components are generally significantly attenuated and the resolution impaired. Diffuse optical tomography has been used for quantitative imaging of absorption and scattering [41, 42, 43, 44, 45, 46] as well as concentration and fluorochrome lifetime measurements with simulated or phantom measurements [47, 48, 49, 50, 51, 52]. Recently, DOT has been applied clinically for imaging tissue oxy- and deoxy-hemoglobin concentration and blood saturation [53, 54, 55] and contrast agent uptake in absorption mode [56].

A particular development that facilitates in vivo molecular interrogations of tissue is the use of fluorescence molecular tomography (FMT) [20]. The method produces quantified three-dimensional reconstructions of fluorescence activation or concentration using measurements of fluorescent molecular probes at both the emission and excitation wavelengths. The theoretical mainframe has been described elsewhere [52]. The main advantage of using both intrinsic and fluorescence contrast is that no absolute photon-field measurements are required, yet absolute fluorochrome concentrations can be reconstructed. Furthermore, the method does not require any measurements obtained before contrast agent administration, which is a crucial parameter for in vivo imaging of probes that require long circulation times to achieve sufficient accumulation in their intended targets.

FMT imaging systems

In order to perform fluorescence tomography, tissue has to be illuminated at different projections and multiple measurements should be collected from the boundary of the tissue of investigation. FMT, in its simplest imple-

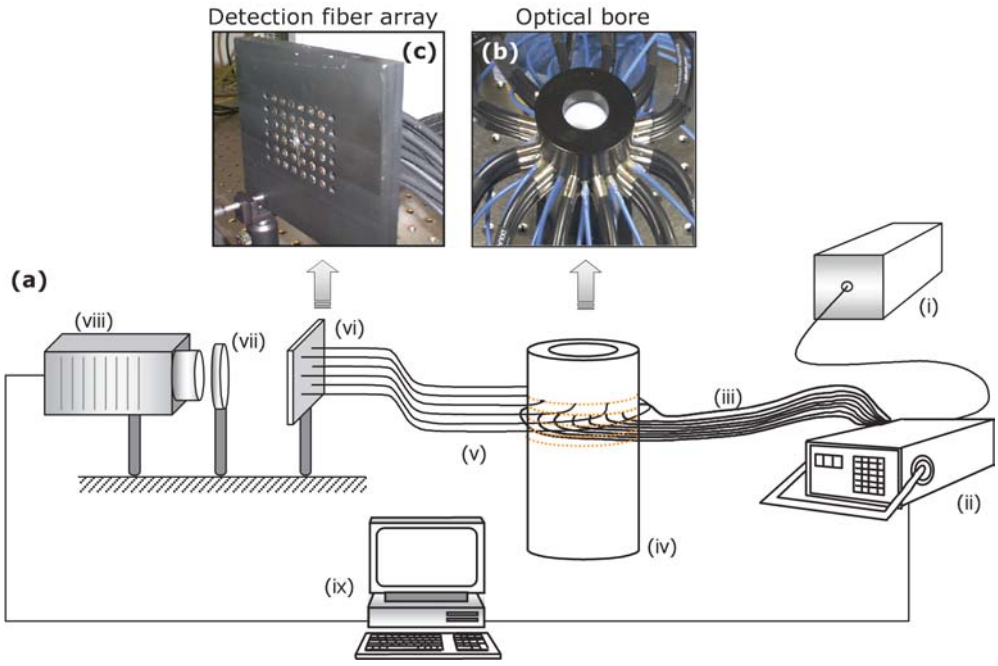

Fig. 9a–c Example of an FMT scanner. **a** The scanner uses multiple sources and detectors to effectively collect light measurement at multiple projections around the animal's body. For details see text. **b** Photograph of the optical bore used for animal investigations. The source fibers (*blue*) and detection fiber bundles (*black*) are shown installed. **c** Photograph of the fiber bundle array arranged for imaging by the CCD camera

mentation, needs only measurements of fluorescence and intrinsic light using constant-wave sources in order to resolve the single quantity targeted, namely fluorochrome concentration. This is in contrast to DOT which, in its general form, requires decomposition of absorption from scattering and therefore requires more elaborate photon technologies such as intensity-modulated sources or short photon pulses and appropriate detection systems. The ability of FMT to operate with constant wave systems allows for a practical and relatively inexpensive implementation of multiple detection channels using CCD cameras. In CW mode, CCD cameras offer very high sensitivity and low noise levels. Nevertheless, the use of advanced photon sources and detection systems can enhance tomographic performance by potentially improving resolution and resolving lifetime as well [48, 49].

A CCD-based FMT system example is shown in Fig. 9a. The light source (i) is generally a laser diode at the appropriate wavelength to excite the targeted fluorochrome. Multiple laser diodes at different wavelengths could be combined in the same system (either by time sharing or spectral separation) to excite multiple fluorochromes simultaneously. The light from the laser diode can be directed to an optical switch (ii) for time sharing one input to many outputs and directed with optical fibers (iii) at different points around the body of investigation or a specially designed "optical bore" (iv). Our implementation of an optical bore [57] is shown in Fig. 9b. The optical bore contains the body of examination similar to a CT or MR scanner. Typically, such an implementation would require the animal immersed into a "matching fluid" (also shown in Fig. 9b contained in the bore), such as a water solution of a scatterer (e.g., TiO_2 particles) and an absorber (India Ink or similar) that matches the optical properties of the tissue investigated. The matching fluid serves virtually the same function as gel to ultrasound. Fiber bundles (v) can be used to collect photons through the turbid medium and direct them onto the CCD camera (viii) either by direct fiber coupling or by an appropriate positioning arrangement (vi) so that the fiber output can be imaged via a lens system as depicted in Fig. 9c. Appropriate filters (vii) are necessary to reject background ambient light and intrinsic or fluorescence signals according to the measurement performed. A reference measurement could also be introduced to account for temporal variations in laser intensity. The use of an optical bore and matching fluid is a convenient approach for matching photons onto tissue but by no means limiting. Different schemes, including direct fiber positioning on the tissue surface, at arbitrary geometries, including geometries, that could be used by endoscopic probes could be devised.

In vivo imaging

The FMT has been used recently for imaging of cathepsin B activity within deep structures. Figure 10 shows a representative experiment of the results obtained from 9L gliosarcomas stereotactically implanted into unilateral brain hemispheres of nude mice, as cathespin B activity had been implicated in glioma invasion [58, 59, 60]. Correlative MR imaging was performed to determine the

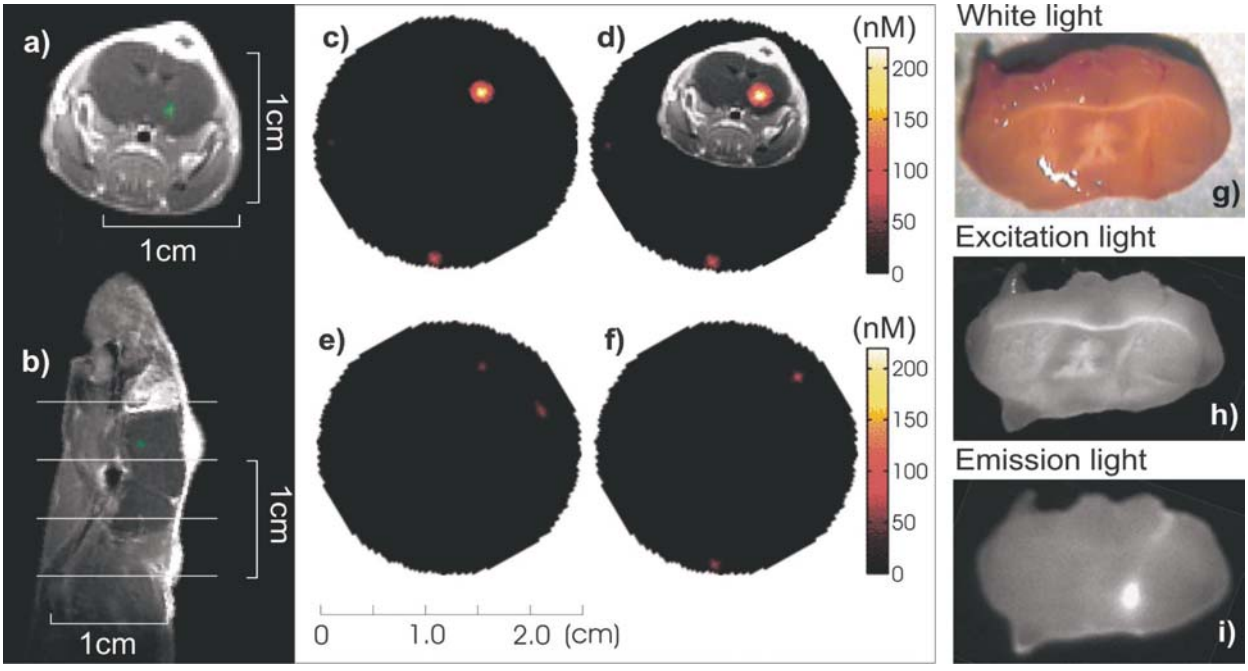

Fig. 10a–i In-vivo FMT of cathepsin B expression levels in 9L gliosarcomas stereotactically implanted into unilateral brain hemispheres of nude mice. **a**, **b** Axial and sagittal MR slices of an animal implanted with a tumor, which is shown in green after gadolinium enhancement. **c**, **e**, **f**, Consecutive FMT slices obtained from top to bottom from the volume of interest shown in **b** by *thin white horizontal lines*. **d** Superposition of the MR axial slice passing through the tumor **a** onto the corresponding FMT slice **c** after appropriately translating the MR image to the actual dimensions of the FMT image. **g**, **h** Axial brain section through the 9L tumor imaged with white light and with monochromatic light at the excitation wavelength (675 nm), respectively, and **i** fluorescence image of the same axial brain section demonstrating a marked fluorescent probe activation, congruent with the tumor position identified by gadolinium-enhanced MRI and FMT. (Reproduced from [20])

presence and location of tumors prior to the FMT imaging studies. Figure 10a and b depicts the gadolinium-enhanced tumor (enhancement is shown in a green color map superimposed onto a T1-weighted image) on axial (Fig. 10a) and sagittal (Fig. 10b) slices. Figure 10c, e, and f depicts the three consecutive FMT slices obtained from top to bottom of the volume of interest. The location and volume covered by the three slices is indicated in Fig. 10b by thin white horizontal lines. Figure 10c shows marked local probe activation relative to adjacent slices, congruent with the location of the tumor identified on the MR images. Figure 10d shows a superposition of the MR axial slice passing through the tumor (Fig. 10a) onto the corresponding FMT slice (Fig. 10c) after appropriately translating the MR image to the actual dimensions of the FMT image. For coregistration purposes we used special water-containing fiducials and body marks that facilitated matching of the MR and FMT orientation and animal positioning. The in vivo imaging data correlated well with surface-weighted reflectance imaging of the excised brain. Figure 10g depicts the axial brain section through the 9L tumor examined with white light using a CCD camera mounted onto a dissecting microscope, Fig. 10h shows the same brain section imaged using a previously developed reflectance imaging system [14] at the excitation wavelength (675 nm), and Fig. 10i is the fluorescence image obtained at the emission light wavelength using appropriate three-cavity cut-off filters that demonstrates a marked fluorescent probe activation, congruent with the tumor position identified by gadolinium-enhanced MRI and FMT. The above results confirm that cathepsin B can be used as an imaging marker [25] since the protease is produced in considerable amounts by tumor cells and by recruited host cells [61]. Cathepsin B expression in the tumors was further confirmed by immunohistochemistry, Western blotting and RT-PCR.

Quantification: resolution and coregistration

The feasibility to three-dimensionally reconstruct and quantify fluorochromes embedded in diffuse media has been demonstrated in the past [47, 48, 49, 52]. It has been further shown that FMT can yield linear responses over a wide area of physiologically relevant fluorochrome concentrations [57]. Figure 11 depicts reconstructions obtained for the range 1–800 nM concentration of the Cy5.5 fluorochrome obtained with a system similar to the one shown in Fig. 9. The geometry employed is shown in Fig. 11a. A 2-mm radius tube was

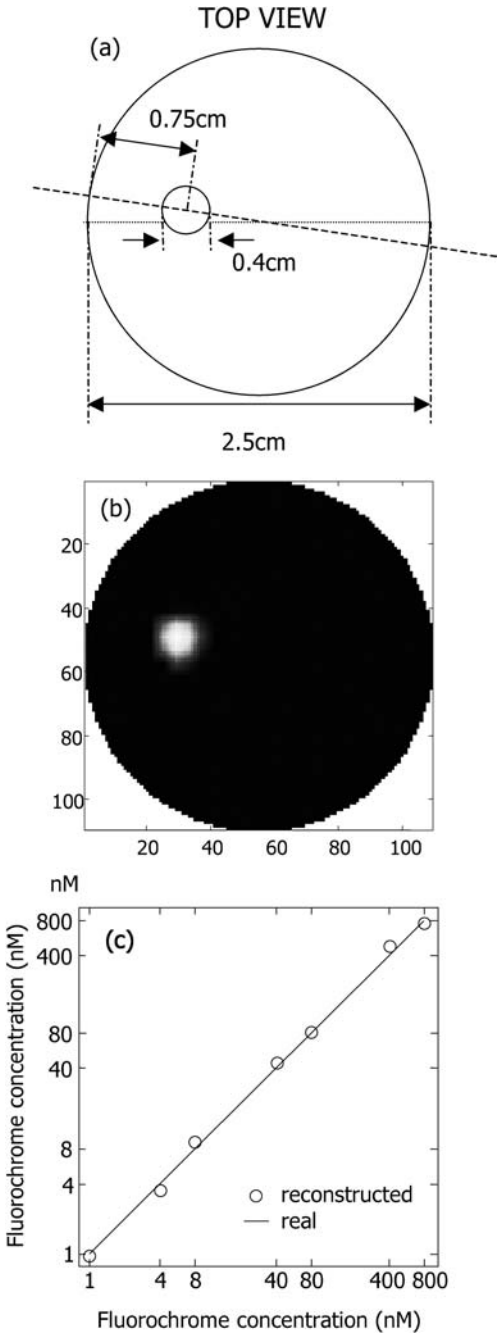

Fig. 11a–c Reconstruction linearity for varying fluorochrome concentrations. **a** Experimental phantom used for the demonstration. The *small circle* represents a tube of 100 μl volume containing different concentrations of Cy5.5 dye. **b** Typical image reconstructed. **c** Reconstructed vs real fluorochrome concentration. The linearity achieved spans more than two orders of magnitude of biologically relevant fluorochrome concentrations. (Adapted from [57])

immersed into the optical bore (shown in Fig. 9) and contained various concentrations of fluorochromes. A typical reconstructed image is seen in Fig. 11b. Figure 11c plots the reconstructed fluorochrome concentration as a function of the expected concentration. The reconstructed value demonstrates a remarkably linear response for the whole range of examined concentrations [57].

The resolution limits of diffuse light imaging techniques have been studied theoretically, but there is limited experimental demonstration, mainly due to the lack of high source-detection efficiency systems. Increasing the number of sources and detectors improves resolution not only due to the higher spatial sampling but also due to the improvements in signal-to-noise ratio achieved in increased data sets [62]. Naturally, improvements of source and detector density do not scale linearly with resolution improvements. It is expected that the resolution for small animal imaging would be of the order of 1–2 mm, whereas for larger tissues it would approach 4–5 mm [62].

The FMT can be combined with high-resolution "reflectance" imaging in superimposing surface architectural features and markers on the underlying three-dimensional reconstruction to correlate the tomographic results with anatomical features, especially in animal imaging. Such an example is shown in Fig. 12. Figure 12a depicts a merged axial FMT/MRI image obtained from the nude mouse shown in Fig. 2. Figure 12b depicts the sagittal MRI image of the same animal and the three FMT slices imaged. Figure 12c depicts a three-dimensional rendering of the superposition of the three-dimensional FMT images with the two dimensional intrinsic light image (shown in Fig. 2b) after application of appropriate thresholds. Furthermore, the combination of FMT with high-resolution imaging methods that primarily target structure, such as X-ray CT or MRI, could yield a superior hybrid imaging modality in which highly sensitive molecular information and high resolution is achieved. Such an approach is feasible due to the optical component compatibility with most other medical imaging modalities and has been recently applied to performing clinical investigations of the breast using a combined MRI and DOT system [19].

Clinical feasibility of fluorescence imaging

Clinical fluorescent imaging would require detection of fluorescent signals that have propagated for several centimeters into tissue. Figure 13a demonstrates the photon attenuation rate of different human tissues. In particular, it is shown that breast tissue and the adult lung attenuates NIR light one order of magnitude every 2.5 cm, the attenuation rate in denser breast approaches one order

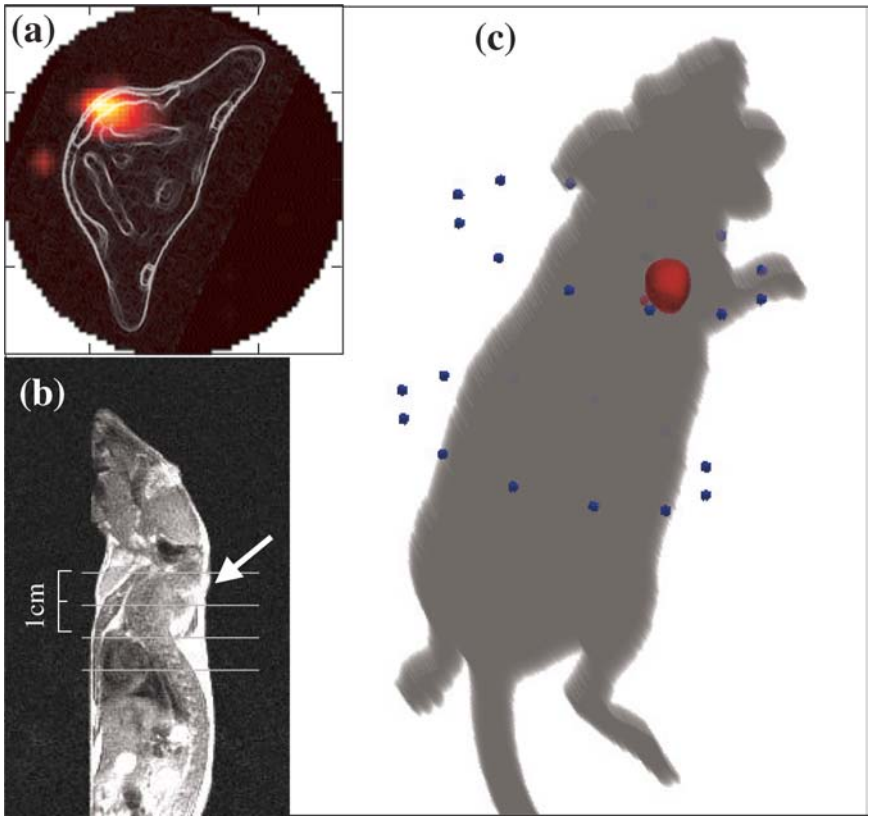

Fig. 12a–c An example of merging two-dimensional with three-dimensional information for improving visualization. **a** The FMT image of the mouse shown in Fig. 2. **b** An MRI sagittal image. The three-plane FMT images are contained between the *white horizontal lines*. The *arrow* indicates the position of the tumor. **c** Rendering of the FMT volumetric reconstruction superimposed with the two-dimensional intrinsic light image after application of appropriate thresholds

of magnitude every 1.5 cm and the attenuation rate in brain and muscle is approximately one order of magnitude every 1.0 cm. In signal strength terms Fig. 13 plots fluorescence counts per second of exposure and square millimeter of of CCD detector area, as a function of organ diameter. This calculation is for a tumor-like lesion of 100 µl volume and 100 nM of Cy5.5 concentration (10 pico-moles) located near the center of the various organs simulated. The simulation is based on experimental measurements obtained from a diffuse volume (similar to the one shown on Fig. 11a but with varying outer diameter) using 30 mW of illuminating power [22].

There are also three horizontal lines plotted, marking the 10-, 20-, and 30-dB signal-to-noise ratio (SNR) achieved assuming shot-noise limited detection. In reality, background fluorescence (primarily due to non-specific dye distribution) limits the SNR achieved, since background signals can be seen as "biologically induced

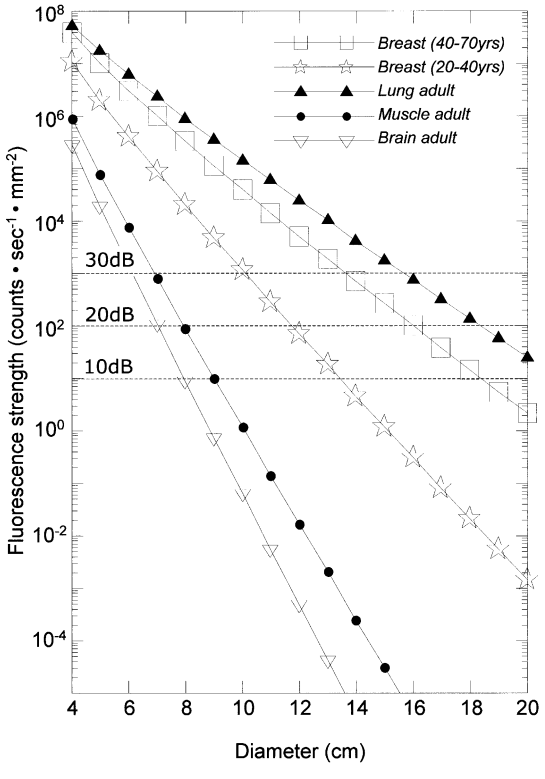

Fig. 13 Average fluorescent photon counts expected at the periphery of different organs due to a fluorochrome located 0.5 cm off center as a function of organ diameter. Three signal-to-noise levels for shot-noise limited detection are also plotted. (From [22])

noise" after appropriate subtraction schemes [63]. Data set optimization [62] and appropriate algorithms [64] can be used to image at low SNR and such considerations should be addressed on a case-to-case basis. This study, however, demonstrates that fluorescence imaging of human tissues becomes an issue of uptake-to-background contrast rather than of propagation feasibility. Important to the latter argument is that fluorescence offers mechanisms for multifold background suppression by using quenching and activation (dequenching) of fluorescent probes [25, 65] or fluorescence resonance energy transfer [66]. These technologies significantly minimize background signals in vivo and, combined with advances in drug delivery and hardware improvements, could surpass the predictions of this study.

Conclusion

Despite advances in medical imaging technologies over the past two decades, we are currently still limited in our ability to detect tumors or other diseases in their earliest stage of formation, phenotype tumors during complex cycles of growth, invasion and metastases, to use imaging techniques to speed up drug testing, and to use imaging as an objective endpoint for tailoring therapies in a given individual. Similar limitations also exist in neurodegenerative, cardiovascular, and immunologic diseases. Traditional cross-sectional imaging techniques, such as MR, CT, and ultrasound, primarily rely on physical (e.g., proton density, relaxation times, absorption, scattering) and/or occasionally physiological parameters as the main source of image signal. We describe herein a new set of technologies that could allow imaging of specific molecular markers in vivo. This has been enabled by several developments:

1. The development of "smart" and targeted fluorescent molecular probes developed for an increasing number of targets identified by gene-array profiles
2. Miniaturization and development of highly sensitive imaging equipment that allows recording of fluorescent signals at pico- to femto-mole accumulations
3. The ability to produce tomographic images of near-infrared probe distribution in whole bodies

The technology has been currently applied to imaging small animals, but it could be expanded to clinical use as well, due to the penetration of near-infrared fluorescent signals for several centimeters in tissues. Furthermore, the optical technology is relatively inexpensive, can be made portable, and uses non-ionizing radiation and stable molecular markers. These features can allow easy laboratory and bench-top use and enable monitoring of molecular events repeatedly and over time. The combination of molecular beacons and optical imaging technologies is expected to play a fundamental role in biomedicine in the next decade and continued developments in probe design and imaging technologies will undoubtedly further expand current capabilities.

References

1. Chance B (1991) Optical method. Annu Rev Biophys Biophys Chem 20:1–28
2. Weissleder R (2001) A clearer vision for in vivo imaging. Nat Biotechnol 19:316–317
3. Ntziachristos V, Chance B (2001) Probing physiology and molecular function using optical imaging: applications to breast cancer. Breast Cancer Res 3:41–46
4. Korlach J, Schwille P, Webb WW et al. (1999) Characterization of lipid bilayer phases by confocal microscopy and fluorescence correlation spectroscopy. Proc Natl Acad Sci 96:8461–8466
5. Rajadhyaksha M, Grossman M, Esterowitz D et al. (1995) In vivo confocal scanning laser microscopy of human skin: melanin provides strong contrast. J Invest Dermatol 104:946–952
6. Gonzalez S, Rajadhyaksha M, Rubinstein G et al. (1999) Characterization of psoriasis in vivo by reflectance confocal microscopy. J Med 30:337–536
7. Konig K (2000) Multiphoton microscopy in life sciences. J Microsc 200:83–104
8. Buehler C, Kim KH, Dong CY et al. (1999) Innovations in two-photon deep tissue microscopy. IEEE Eng Med Biol Mag 18:23–30
9. So PT, Dong CY, Masters BR et al. (2000) Two-photon excitation fluorescence microscopy. Annu Rev Biomed Eng 2:399–429
10. Masters BR, So PT, Gratton E (1997) Multiphoton excitation fluorescence microscopy and spectroscopy of in vivo human skin. Biophys J 72:2405–2412
11. Dellian M, Yuan F, Trubetskoy VS et al. (2000) Vascular permeability in a human tumour xenograft: molecular charge dependence. Br J Cancer 82:1513–1518
12. Monsky WL, Fukumura D, Gohongi T et al. (1999) Augmentation of transvascular transport of macromolecules and nanoparticles in tumors using vascular endothelial growth factor. Cancer Res 59:4129–4135
13. Toomre D, Manstein DJ (2001) Lighting up the cell surface with evanescent wave microscopy. Trends Cell Biol 11:298–303
14. Mahmood U, Tung CH, Bogdanov A et al. (1999) Near infrared optical imaging system to detect tumor protease activity. Radiology 213:866–870
15. Becker A, Hessenius C, Licha K et al. (2001) Receptor-targeted optical imaging of tumors with near-infrared fluorescent ligands. Nat Biotechnol 19:327–331
16. Yang M, Baranov E, Jiang P et al. (2000) Whole-body optical imaging of green fluorescent protein-expressing tumors and metastases. Proc Natl Acad Sci USA 97:1206–1211

17. Zaheer A, Lenkinski RE, Mahmood A et al. (2001) In vivo near-infrared fluorescence imaging of osteoblastic activity. Nat Biotechnol 19:1148–1154
18. Reynolds JS, Troy TL, Mayer RH et al. (1999) Imaging of spontaneous canine mammary tumors using fluorescent contrast agents. Photochem Photobiol 70:87–94
19. Ntziachristos V, Yodh AG, Schnall M et al. (2000) Concurrent MRI and diffuse optical tomography of breast after indocyanine green enhancement. Proc Natl Acad Sci USA 97:2767–2772
20. Ntziachristos V, Tung C, Bremer C et al. (2002) Fluorescence-mediated tomography resolves protease activity in vivo. Nat Med 8:757–760
21. Chance B, Kang K, He L et al. (1993) Highly sensitive object location in tissue models with linear in-phase and anti-phase multi-element optical arrays in one and two dimensions. Proc Natl Acad Sci USA 90:3423–3427
22. Ntziachristos V, Ripoll J, Weissleder R (2002) Would near-infrared fluorescence signals propagate through large human organs for clinical studies. Opt Lett 27:527–529
23. Contag CH, Jenkins D, Contag PR et al. (2000) Use of reporter genes for optical measurements of neoplastic disease in vivo. Neoplasia 2:41–52
24. Ramanujam N, Chen J, Gossage K et al. (2001) Fast and noninvasive fluorescence imaging of biological tissues in vivo using a flying-spot scanner. IEEE Trans Biomed Eng 48:1034–1041
25. Weissleder R, Tung CH, Mahmood U et al. (1999) In vivo imaging of tumors with protease-activated near-infrared fluorescent probes. Nat Biotech 17:375–378
26. Tung CH, Mahmood U, Bredow S et al. (2000) In vivo imaging of proteolytic enzyme activity using a novel molecular reporter. Cancer Res 60:4953–4958
27. Bremer C, Tung C, Weissleder R (2001) Imaging of metalloproteinase2 inhibition in vivo. Nat Med 7:743–748
28. Bremer C, Bredow S, Mahmood U et al. (2001) Optical imaging of matrix metalloproteinase-2 activity in tumors: feasibility study in a mouse model. Radiology 221:523–529
29. Achilefu S, Dorshow RB, Bugaj JE et al. (2000) Novel receptor-targeted fluorescent contrast agents for in vivo tumor imaging [in process citation]. Invest Radiol 35:479–485
30. Bugaj JE, Achilefu S, Dorshow RB et al. (2001) Novel fluorescent contrast agents for optical imaging of in vivo tumors based on a receptor-targeted dye-peptide conjugate platform. J Biomed Opt 6:122–133
31. Wouters FS, Verveer PJ, Bastiaens PI (2001) Imaging biochemistry inside cells. Trends Cell Biol 11:203–211
32. Contag CH, Spilman SD, Contag PR et al. (1997) Visualizing gene expression in living mammals using a bioluminescent reporter. Photochem Photobiol 66:523–531
33. Sweeney TJ, Mailander V, Tucker AA et al. (1999) Visualizing the kinetics of tumor-cell clearance in living animals. Proc Natl Acad Sci 96:12044–12049
34. Mahmood U, Tung CH, Tang Y et al. (in press) Feasibility of in-vivo multi-channel optical imaging of gene expression: an experimental study in mice. Radiology
35. Schotland J-C (1997) Continuous wave diffusion imaging. J Opt Soc Am 14:275–279
36. Yodh AG, Chance B (1995) Spectroscopy and imaging with diffusing light. Phys Today 48:34–40
37. Hielscher AH, Klose AD, Hanson KM (1999) Gradient-based iterative image reconstruction scheme for time-resolved optical tomography. IEEE Trans Med Imaging 18:262–271
38. Barbour RL, Graber HL, Chang JW et al. (1995) MRI-guided optical tomography: prospects and computation for a new imaging method. IEEE Comput Sci Eng 2:63–77
39. Colak SB, van der Mark MB, Hooft GW et al. (1999) Clinical optical tomography and NIR spectroscopy for breast cancer detectio. IEEE J Selected Top Quantum Electron 5:1143–1158
40. Arridge SR (1999) Optical tomography in medical imaging. Inverse Prob 15:R41–R93
41. Oleary MA, Boas DA, Chance B et al. (1995) Experimental images of heterogeneous turbid media by frequency-domain diffusing-photon tomography. Opt Lett 20:426–428
42. Jiang HB, Paulsen KD, Osterberg UL et al. (1998) Improved continuous light diffusion imaging in single- and multi-target tissue-like phantoms. Phys Med Biol 43:675–693
43. Chang JW, Graber HL, Koo PC et al. (1997) Optical imaging of anatomical maps derived from magnetic resonance images using time-independent optical sources. IEEE Trans Med Imaging 16:68–77
44. Ntziachristos V, Ma XH, Chance B (1998) Time-correlated single photon counting imager for simultaneous magnetic resonance and near-infrared mammography. Rev Sci Instrum 69:4221–4233
45. Pogue BW, Testorf M, McBride T et al. (1997) Instrumentation and design of a frequency domain diffuse optical tomography imager for breast cancer detection. Opt Expr 1:391–403
46. Schmitz CH, Graber HL, Barbour RL (2000) A fast versatile instrument for dynamic optical tomography. In: Advances in optical imaging and photon migration, OSA. Technical Digest. Optical Society of America, Washington DC, pp 94–96
47. Chang JH, Graber HL, Barbour RL (1997) Imaging of fluorescence in highly scattering media. IEEE Trans Biomed Eng 44:810–822
48. Oleary MA, Boas DA, Li XD et al. (1996) Fluorescence lifetime imaging in turbid media. Opt Lett 21:158–160
49. Paithankar DY, Chen AU, Pogue BW et al. (1997) Imaging of fluorescent yield and lifetime from multiply scattered light reemitted from random media. Appl Opt 36:2260–2272
50. Chernomordik V, Hattery D, Gannot I et al. (1999) Inverse method 3-D reconstruction of localized in vivo fluorescence: application to Sjogren syndrome. IEEE J Selected Top Quantum Electron 5:930–935
51. Sevick-Muraca EM, Lopez G, Reynolds JS et al. (1997) Fluorescence and absorption contrast mechanisms for biomedical optical imaging using frequency-domain techniques. Photochem Photobiol 66:55–64
52. Ntziachristos V, Weissleder R (2001) Experimental three-dimensional fluorescence reconstruction of diffuse media using a normalized Born approximation. Opt Lett 26:893–895
53. Pogue BW, Poplack SP, McBride TO et al. (2000) Hemoglobin imaging of breast tumors with near-infrared tomography. Radiology 214:G05H
54. Hillman EMC, Hebden JC, Schweiger M et al. (2001) Time resolved optical tomography of the human forearm. Phys Med Biol 46:1117–1130
55. Benaron DA, Hintz SR, Villringer A et al. (2000) Noninvasive functional imaging of human brain using light. J Cereb Blood Flow Metab 20:469–477
56. Ntziachristos V (2000) Concurrent diffuse optical tomography, spectroscopy and magnetic resonance of breast cancer. University of Pennsylvania
57. Ntziachristos V, Weissleder R (2002) CCD-based scanner for three-dimensional fluorescence-mediated diffuse optical tomography of small animals. Med Phys 29:803–809

58. Demchik LL, Sameni M, Nelson K et al. (1999) Cathepsin B and glioma invasion. Int J Dev Neurosci 17:483–494
59. Yan S, Sameni M, Sloane BF (1998) Cathepsin B and human tumor progression. Biol Chem 379:113–123
60. Rempel SA, Rosenblum ML, Mikkelsen T et al. (1994) Cathepsin B expression and localization in glioma progression and invasion. Cancer Res 54:6027–6031
61. Koblinski JE, Ahram M, Sloane BF (2000) Unraveling the role of proteases in cancer. Clin Chim Acta 291:113–135
62. Culver J, Ntziachristos V, Holboke M et al. (2001) Optimization of optode arrangements for diffuse optical tomography: a singular value analysis. Opt Lett 26:701–703
63. Wu J, Perelman L, Dasari RR et al. (1997) Fluorescence tomographic imaging in turbid media using early-arriving photons and Laplace transforms. Proc Natl Acad Sci USA 94:8783–8788
64. Eppstein MJ, Dougherty DE, Troy TL et al. (1999) Biomedical optical tomography using dynamic parameterization and Bayesian conditioning on photon migration measurements. Appl Opt 38:2138–2150
65. Tyagi S, Kramer FR (1996) Molecular beacons: probes that fluoresce upon hybridization. Nat Biotechnol 14:303–308
66. Tyagi S, Marras SAE, Kramer FR (2000) Wavelength-shifting molecular beacons. Nat Biotechnol 18:1191–1196